Video Article

Synthesis of Non-uniformly Pr-doped $SrTiO_3$ Ceramics and Their Thermoelectric Properties

Arash Mehdizadeh Dehkordi[1], Sriparna Bhattacharya[2], Taghi Darroudi[3], Xiaoyu Zeng[2], Husam N. Alshareef[4], Terry M. Tritt[1,2]

[1]Department of Materials Science and Engineering, Clemson University

[2]Department of Physics and Astronomy, Clemson University

[3]Electron Microscope Facility, Clemson University

[4]Materials Science and Engineering, King Abdullah University of Science and Technology

Correspondence to: Arash Mehdizadeh Dehkordi at amehdiz@g.clemson.edu

URL: http://www.jove.com/video/52869
DOI: doi:10.3791/52869

Keywords: Chemistry, Issue 102, Oxide Thermoelectrics, Praseodymium, $SrTiO_3$, Enhanced Figure of Merit, Enhanced Power Factor, N-type Semiconductor, Mobility Enhancement, Grain Boundary Engineering

Date Published: 8/15/2015

Citation: Mehdizadeh Dehkordi, A., Bhattacharya, S., Darroudi, T., Zeng, X., Alshareef, H.N., Tritt, T.M. Synthesis of Non-uniformly Pr-doped $SrTiO_3$ Ceramics and Their Thermoelectric Properties. *J. Vis. Exp.* (102), e52869, doi:10.3791/52869 (2015).

Abstract

We demonstrate a novel synthesis strategy for the preparation of Pr-doped $SrTiO_3$ ceramics via a combination of solid state reaction and spark plasma sintering techniques. Polycrystalline ceramics possessing a unique morphology can be achieved by optimizing the process parameters, particularly spark plasma sintering heating rate. The phase and morphology of the synthesized ceramics were investigated in detail using X-ray diffraction, scanning electron microcopy and energy-dispersive X-ray spectroscopy. It was observed that the grains of these bulk Pr-doped $SrTiO_3$ ceramics were enhanced with Pr-rich grain boundaries. Electronic and thermal transport properties were also investigated as a function of temperature and doping concentration. Such a microstructure was found to give rise to improved thermoelectric properties. Specifically, it resulted in a significant improvement in carrier mobility and the thermoelectric power factor. Simultaneously, it also led to a marked reduction in the thermal conductivity. As a result, a significant improvement (> 30%) in the thermoelectric figure of merit was achieved for the whole temperature range over all previously reported maximum values for $SrTiO_3$-based ceramics. This synthesis demonstrates the steps for the preparation of bulk polycrystalline ceramics of non-uniformly Pr-doped $SrTiO_3$.

Video Link

The video component of this article can be found at http://www.jove.com/video/52869/

Introduction

Oxide thermoelectrics were shown to be promising candidates for high-temperature thermoelectric applications, from stability and cost perspectives to electronic transport properties. Among the n-type oxide thermoelectrics, highly doped strontium titanate (STO) has attracted much attention due to its intriguing electronic properties. However, a large total thermal conductivity ($\kappa \sim 12$ W m^{-1} K^{-1} at 300 K for single crystals)[1] and a low carrier mobility ($\mu \sim 6$ cm^2 V^{-1} sec^{-1} at 300 K for single crystals)[1] detrimentally affect the thermoelectric performance which is evaluated by a dimensionless figure of merit, $ZT = \alpha^2\sigma T/\kappa$, where α is the Seebeck coefficient, σ the electrical conductivity, T the absolute temperature in Kelvin, and κ the total thermal conductivity. We herein define the numerator as the power factor, $PF = \alpha^2\sigma T$. In order for this oxide thermoelectric material to compete with other high-temperature thermoelectrics (such as SiGe alloys), a more pronounced increase in the power factor and/or decrease in lattice thermal conductivity are required.

The majority of the experimental studies in order to improve the thermoelectric properties of STO have mainly focused on the reduction of thermal conductivity through strain-field and mass fluctuation scattering of phonons. These attempts include: (i) Single- or double-doping of the Sr^{2+} and/or Ti^{4+} sites, as the main efforts with respect to this direction,[2,3] (ii) Synthesis of natural superlattice Ruddlesden–Popper structures in order to further reduce the thermal conductivity through insulating SrO layers,[4] and (iii) Composite engineering by addition of a nanosized second phase.[5] However, up until recently, no enhancement strategy has been reported to substantially increase the thermoelectric power factor in these oxides. The reported maximum power factor (PF) values in bulk single- and poly-crystalline STO have been confined to an upper limit of $PF < 1.0$ W m^{-1} K^{-1}.

A variety of synthesis approaches and processing techniques have been employed to implement the ideas attempted above. The powder synthesis routes include conventional solid-state reaction,[6] sol-gel,[7] hydrothermal,[8] and combustion synthesis,[9] whereas conventional sintering,[6] hot pressing[10] and recently spark plasma sintering[12] are among the common techniques used to densify the powders into bulk ceramics. However, for a similar dopant (*e.g.,* La) and doping concentration, the resulting bulk ceramics exhibit a range of electronic and thermal transport properties. This is in large due to the strongly process-dependent defect chemistry of $SrTiO_3$ which results in synthesis-dependent properties. There is only a handful of reports optimizing the synthesis and processing parameters to benefit thermoelectric transport. It is worth mentioning

that due to the very small phonon mean free path in $SrTiO_3$ (l_{ph}~2 nm at 300 K),[11] nanostructuring is not a viable option for the improvement of the TE performance of bulk STO ceramics primarily through the reduction of the lattice thermal conductivity.

Recently, we reported more than 30% improvement in the thermoelectric figure of merit in non-uniformly Pr-doped $SrTiO_3$ ceramics originating from a simultaneously enhanced thermoelectric power factor and reduced thermal conductivity.[12,13] In this detailed video protocol, we present and discuss the steps of our synthesis strategy for the preparation of these Pr-doped STO ceramics exhibiting improved electronic and thermoelectric properties.

Protocol

1. Preparation of Pr-doped $SrTiO_3$ Powder

1. In order to prepare 10 g of $Sr_{0.95}Pr_{0.05}TiO_3$ powder, weigh the stoichiometric amounts of $SrCO_3$ powder (7.53407 g), TiO_2 nanopowder (4.28983 g), and Pr_2O_3 sintered lump (0.44299 g) following the reaction for x = 0.05:

$$(1-x)SrCO_3 + \left(\frac{x}{2}\right) Pr_2O_3 + TiO_2 \rightarrow Sr_{1-x}Pr_xTiO_{3-\delta} + (1-x)CO_2 \qquad (1)$$

2. Grind the weighed Pr_2O_3 sintered lumps to fine particles using an agate mortar and pestle.
3. Add the weighed $SrCO_3$ powder and TiO_2 nanopowder to the Pr_2O_3 and continue grinding and mixing using an agate mortar and pestle until a visually homogenous powder is achieved.
4. Load the ground powder into a glass jar and mix using a turbulator for 30 min to homogenize the mixture.
5. Load the resulting mixed powder into a meticulously cleaned and polished stainless steel die (1 inch in diameter) and sandwich it between two stainless steel plungers.
6. Cold press the powder using a press under an approximately 1 metric ton load.
7. Eject the cold-pressed pellet by placing the die on a hollowed stainless steel cylinder and pushing the plungers and the pellet out from the top using a pushing rod. Upon ejection of the cold pressed pellet (green body) from the die, clean any contamination on the circumferential surface of the pellet by gently covering the pellet with a small piece of scotch-tape and removing a thin layer by ripping the tape.
8. Place the pellet vertically in an alumina boat filled with commercially purchased $SrTiO_3$ powder as the barrier between the alumina boat and the cold press pellet.
9. Place the boat in a tube furnace, heat up to 1,300 °C in 3 hr and keep it at this temperature for 15 hr. Allow the pellet to cool down to RT inside the furnace when the calcination is over. This step is referred to as the “calcination process” thereafter.
10. Grind the pellet using the agate mortar and pestle and load the resulting powder into a glass jar for further mixing using the turbulator.
11. Load the powder into the stainless steel die and cold pressed under an approximately 3 metric tons of load.
12. Repeat the step 1.9 one more time at 1,400 °C in 3 hr and keep it at this temperature for 20 hr.
13. Grind the pellet using the agate mortar and pestle.
14. Repeat steps 1.11, 1.12, and 1.13 one more time for the solid state reaction to reach completion.

2. Preparation of Bulk Polycrystalline Pr-doped $SrTiO_3$ Ceramic

1. Weigh 1.6 g of the as-prepared powder (for a disk 2 mm thick and 12.7 mm in diameter).
2. Prepare circular graphoil pieces to cover the top and bottom interface of the sandwiched powder and graphite plungers in the graphite die. Also, prepare another rectangular graphoil piece to cover the inner wall of the graphite die.
3. Load the as-prepared powder into a graphite die (12.7 mm in inner diameter) and sandwich the powder between two graphite plungers of the same size. Drill a 2-mm hole in the middle of the length of the graphite die and from the outer surface of the die to about 2 mm of the inner surface for temperature reading.
   Note: Adjust the length of the graphite plungers remaining outside the die and position the center of the sandwiched powder cylinder where the hole is placed to get an accurate temperature reading. The faces of the graphite plungers need to be meticulously leveled during the machining of the pieces. Any misalignment can result in the cracking of the sintered pellet during spark plasma sintering.
4. Cold-press the powder gently (load < 200 kg) using a press prior to mounting on the spark plasma sintering plate inside the chamber. Use flat polished stainless steel support plates between the top and bottom plungers and the press stage to avoid damaging the graphite plungers.
5. Wrap a piece of graphite felt around the die for insulation and secure it with graphite yarn. Devise a window on the graphite felt by cutting a rectangular piece of the felt where the temperature reading hole is placed on the die.
6. Place the loaded graphite die and plungers in the spark plasma sintering chamber. Move the stage to the final position.
7. Focus and align the Pyrometer target circle on the temperature reading hole of the die. Make sure the emissivity setting of the pyrometer is set for graphite.
8. Close the chamber and put a 7.7 kN load (approximately 60 MPa) on the sample. Vacuum and purge the chamber with Ar three times and leave the chamber under dynamic vacuum of 6 Pa.
9. Increase the temperature by increasing the current (manually or using a program). Use 250 A min^{-1} (corresponding to approximately 300-400 °C min^{-1}) for the optimized samples. This is the most important step of the spark plasma sintering process.
10. Keep the temperature at 1,500 °C for 5 min by manually adjusting the current or using the program. At the end of the 5 min holding period, shut the current off and quickly release the 7.7 kN load to avoid cracking the sample during the cooling down. Let the sample cool to RT inside the chamber.
11. Release the bulk pellet from the graphite die gently using the cold press. This is done by placing the graphite die on a hollowed steel cylinder and ejecting the pellet and the graphite plungers using a steel pushing rod from the top.
12. Remove the graphoil on top and bottom faces of the pellet as well as the circumferential surface using a sharp razor blade.

13. Polish the sample using a rough sand paper (400 grid) down for 0.3-0.5 mm from each side to assure the complete removal of the graphoil. Clean the sample with acetone.

3. Characterization of Electronic and Thermal Transport Properties of Bulk Ceramics

1. Determine the density of the ceramic disk, ρ, using the Archimedes method.
2. Measure the weight of the sample, W_{dry}, and then the weight of the sample submerged in water, W_{wet}, on a stabilized density measurement system and calculate the Archimedes density from

$$\rho = \frac{W_{\text{dry}}}{W_{\text{dry}} - W_{\text{wet}}} \rho_{\text{water}} \qquad (2)$$

where ρ_{water} is the density of the water at the measurement temperature (*e.g.,* equals 1 g cm^{-3} at 300 K).[14]

2. Measure the thermal diffusivity of the sample, d, using the transient laser-flash technique under a 75 ml min^{-1} flow of Ar. Measure the thickness of the sample, L, accurately first using a digital micrometer.
   Note: Parallel-faced samples with different sizes and shapes (*e.g.,* round discs 12.7 mm in diameter or square 10 x 10 mm^2 disks) and thicknesses between 0.5 and 5 mm can be easily measured.
   1. In the laser-flash thermal diffusivity technique, irradiate one face of the sample by a short (~1 msec) laser pulse and record the temperature rise on the opposite face by an infra-red detector. Then calculate thermal diffusivity by the laser-flash interface software from the thickness of the sample and the temperature rise-time profile using the Parker equation[15]

$$d = 0.138 \frac{L^2}{t_{1/2}} \qquad (3)$$

where *L* is the thickness of the disk and $t_{1/2}$ is the half-time of the maximum temperature rise of the other side of the sample.

Note: The Parker model[15] assumes ideal conditions of adiabatic sample and instantaneous pulse heating, other models have been proposed over the years, which account for various losses in the measurement such as heat losses, finite pulse duration, non-uniform pulse heating and nonhomogeneous structures. We have used the Cowan model[16] with pulse correction which is one of the most advanced methods. It should be noted that in order to maximize the amount of thermal energy transmitted from the front surface and to maximize the signal observed by the IR detector, the sample surfaces must be highly emissive. Usually this requires the application of a thin coating of graphite to the sample surfaces. An uncertainty of 2%-5% in the measurement of thermal diffusivity exists, arising from the determination of dimension.[17]

3. Cut the disk pellet using a diamond saw into rectangular bars, 2 x 2 x 10 mm^3, electrical conductivity and Seebeck coefficient measurements as well as a square disk, 4 x 4 x 1.5 mm^3 for high-temperature specific heat and a thin rectangular piece, 8 x 5 x 1 mm^3 for Hall measurements.
4. Measure the specific heat, C_p, of the sample on the flat and mirror-polished square piece (4 x 4 x 1.5 mm^3) using a differential scanning calorimetry (DSC) under argon flow.[18]
   1. Use a heating rate of 5 K min^{-1} up to 40 °C for an isothermal hold for 10 min to allow the sample to reach thermal equilibrium followed by 20 K min^{-1} heating rate up to 500 °C, with an exact cooling rate which followed. Perform the measurement under the flow of argon (50 ml min^{-1} is suggested).

Note: Due to the sensitivity of the method used for analysis, conduct three measurements to determine the heat capacity including (1) a baseline measurement to subtract the background, (2) measurement of the specific heat of a standard material (such as sapphire) with a known C_P, and (3) measurement of the specific heat of the sample. Ensure that samples are flat and mirror-polished in order to make an ideal contact with the bottom of the measurement crucible (Pt/Rh pans with Al_2O_3 crucibles used in this work). More details on the exact structure of the DSC stage, a comparison of the DSC techniques to others, and exact instructions for measuring a sample can be found in various sources.[19]

5. Calculate the high-temperature thermal conductivity, κ, of the sample from the measured values of thermal diffusivity, *d*, the specific heat, C_P, and the density, *ρ using*[20]

$$\kappa = \rho d C_P. \qquad (4)$$

6. Gold plate the probes contact points (4 contacts) on the 2 x 2 x 10 mm^3 piece cut from the sample to alleviate the contact resistance issues.
   1. In order to sputter gold only on the desired contact areas, wrap a scotch-tape around the 2 x 2 x 10 mm^3 sample to use as a stencil. Leave the 2 x 2 mm^2 faces un-covered. Using a razor blade, cut out 2 very small holes (approximately 1 mm in diameter) in the middle of the 2 x 10 mm^2 face along a line separated by the probes distance.
   2. Sputter a ~ 200 nm-thick gold film using a bench-top gold sputtering unit.[21]

7. Measure the electrical transport properties, namely the electrical conductivity and Seebeck coefficient) of the sample as a function of temperature[22,23].
   1. Measure electrical conductivity using the four-terminal method. Measure the Seebeck coefficient on the same setup using the measurements of temperature and voltage via the two middle thermocouple “probes”. Measure the distance between these two probes using a digital microscope. More details on the electrical transport measurements can be found elsewhere.[22,23]

8. Measure the Hall carrier concentration as a function of temperature on the 8 x 5 x 1 mm^3 sample using a Physical Properties Measurement System.[24]

Representative Results

X-ray diffractions patterns were collected for the as-prepared powders and the corresponding bulk ceramics as a function of Pr-content (**Figure 1**) in order to study the effect of Pr-doping on the $SrTiO_3$ lattice, solubility of Pr in $SrTiO_3$ and the formation of secondary phase(s). The patterns confirm the formation of $SrTiO_3$ phase in all the as-prepared powders where the reflections can be indexed to a cubic lattice with space group (**Figure 1A**). The monotonic change in the indexed lattice parameter from a = 3.906 for x = 0 (undoped) with increasing Pr content confirms the distortion of the lattice upon incorporation of smaller Pr^{3+} ions in Sr^{2+} sites. Weak reflections were also observed for x > 0.05, corresponding to the intermediate praseodymium oxide phase (*e.g.,* Pr_5O_9), which increase intensity with increasing nominal Pr concentration (**Figure 1B**). It was found that by optimizing the SPS heating rate the reflections corresponding to the secondary phase(s) are fully disappeared (**Figure 1C**, **D**).

A synthesis-structure-property relationship study was conducted in order to understand the effect of the SPS heating rate and the observed secondary phase on the electronic transport properties. Scanning electron micrographs were acquired in conjunction with energy-dispersive X-ray spectra to investigate the effect of the synthesis and densification parameters, particularly spark plasma sintering heating rate, on the morphology and the chemistry of the grains and grain boundaries (**Figure 2**). Synthesis-(micro) structure-property relationship was investigated by monitoring the temperature-dependence of electronic transport properties of the bulk ceramics (**Figure 2**). It was found that electrical conductivity can be significantly increased through the optimization of the SPS heating rate (**Figure 2A**). This improvement was attributed to a marked enhancement in the carrier mobility since similar Seebeck coefficient and carrier concentration values were obtained for samples densified under different heating rates (**Figure 2A**, inset). Scanning electron micrographs have shown that the Pr-rich secondary phase present in the as prepared powder (**Figure 2B**, inset) can partially dope the grain boundary region during the SPS process (**Figure 2B**). By the appropriate optimization of the SPS heating rate, the grain boundary region can be fully doped with Pr, in which case an enhancement in the carrier mobility is observed (**Figure 2C**).

Electronic and thermal transport properties of the bulk ceramics prepared with a high SPS heating rate of 300 °C min^{-1} were measured as a function of temperature and Pr content in order to calculate the overall thermoelectric figure of merit (**Figure 3**). All samples exhibit a degenerate semiconducting behavior (*i.e.,* metallic-like) for electrical conductivity (**Figure 3A**) and a corresponding diffusive-like thermopower (**Figure 3B**). Large thermoelectric power factor > 1 W m^{-1} K^{-1} was observed for ceramics with x > 0.075 in a broad temperature range reaching a maximum of 1.3 W m^{-1} K^{-1} for x = 0.15, corresponding to 3 at % Pr (**Figure 3C**). Simultaneously, a monotonic reduction in thermal conductivity was observed with increasing Pr up to x = 0.15 (**Figure 3D**). The optimum nominal Pr concentration was found to be x = 0.15 for these samples.[13] More than 30% improvement in the dimensionless thermoelectric figure of merit (ZT) for the whole temperature range over all previously reported maximum values were achieved as a result of the simultaneous enhancement in the thermoelectric power factor and reduction in the thermal conductivity (**Figure 3E**).[13] Maximum ZT value of 0.35 was obtained at 500 °C. If the measurements are to be performed under a highly reducing atmosphere, maximum ZT values above 0.6 are predicted at 1,000 °C by fitting the experimental electronic and thermal transport data. The possibility of further improvement of the power factor at these temperatures, and hence ZT also exist if the carrier concentration can be further increased.[30]

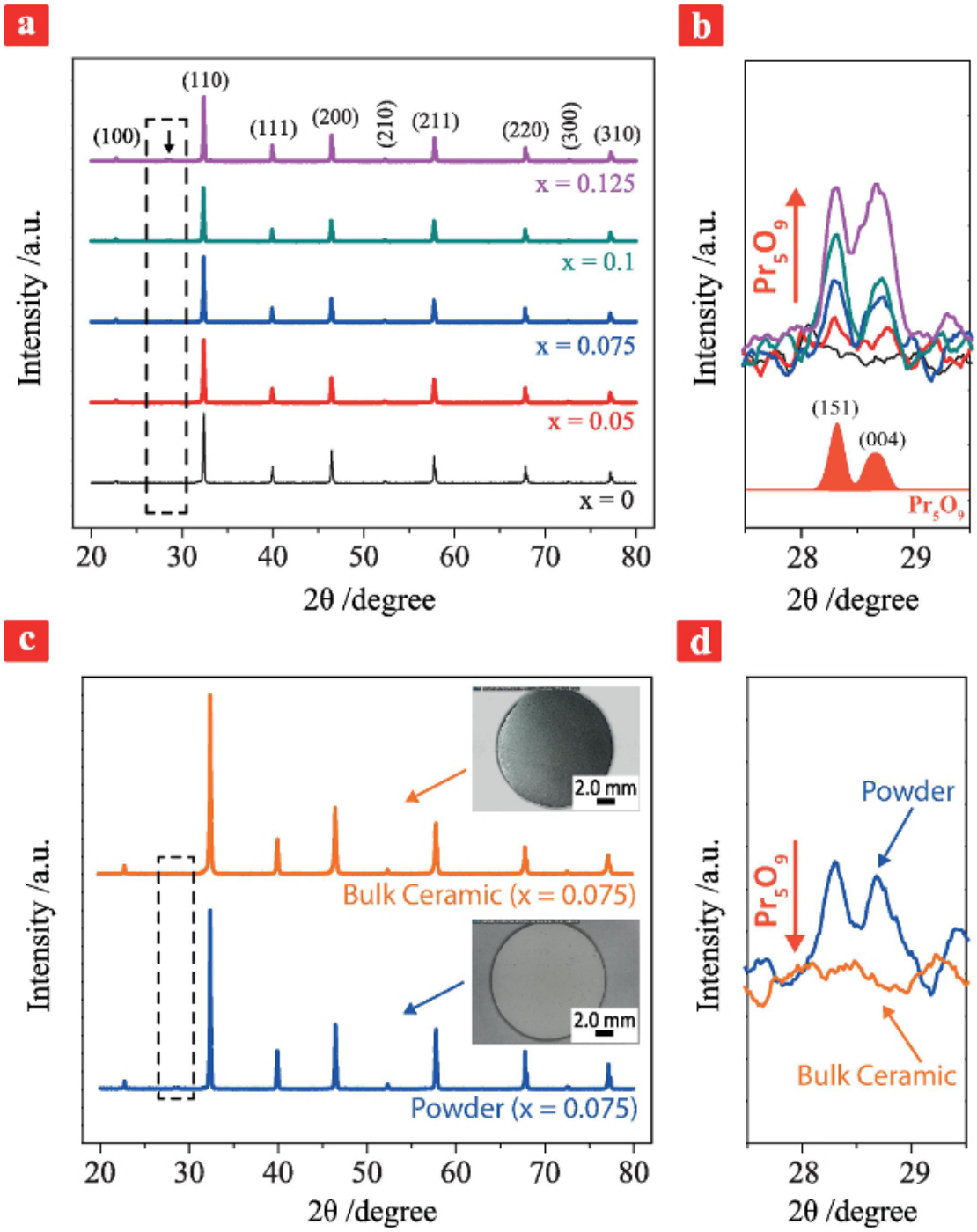

Figure 1. X-ray diffraction profiles. (**A**) X-ray diffraction (XRD) profiles of $Sr_{1-x}Pr_xTiO_{3-\delta}$ powders before SPS as a function of nominal Pr content. (**B**) Magnified view of the dashed rectangle in (a), (**C**) XRD profiles of $Sr_{1-x}Pr_xTiO_{3-\delta}$ with x = 0.075 before SPS (Powder) and after high-heating-rate SPS (Bulk Ceramic). Photographs of cold-pressed powder after solid-state reaction and the corresponding SPSed ceramic are shown. (**D**) Magnified view of the dashed rectangle in (**C**). Reprinted with permission.[12]. Please click here to view a larger version of this figure.

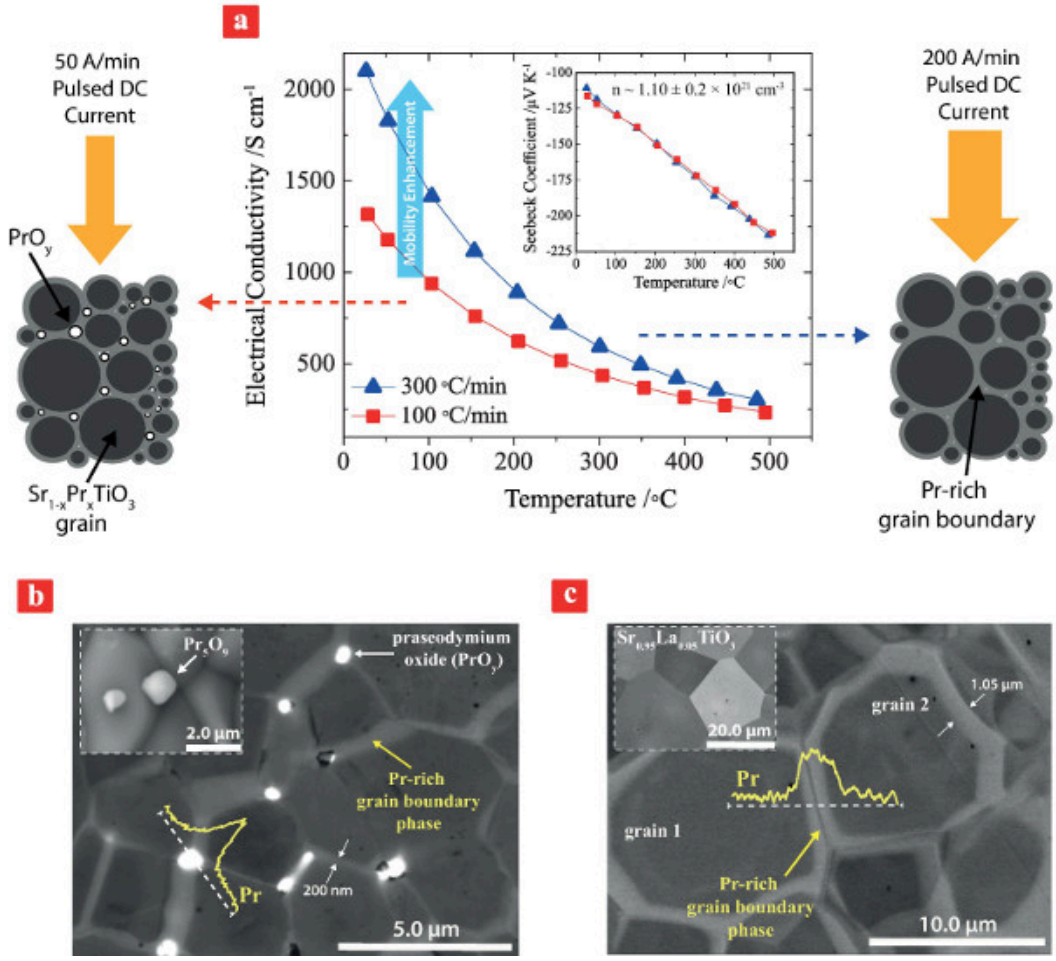

Figure 2. Effect of SPS heating rate. (**A**) Temperature dependence of electrical conductivity and Seebeck coefficient (inset) for $Sr_{1-x}Pr_xTiO_{3-\delta}$ ceramics with x = 0.075 processed using two different SPS heating rates of 100 °C min^{-1} and 300 °C min^{-1}, respectively. (**B**) Backscattered electron (BSE) micrograph of the ceramic made under 100 °C min^{-1} SPS. A typical Pr spectrum of the EDS line scan across a PrO_y particle is shown. (**C**) Backscattered electron micrograph of the ceramic made under a 300 °C min^{-1} SPS heating rate. A typical Pr spectrum of EDS line scan across two grains, grain 1 and grain 2, is shown. The inset depicts the BSE micrograph of the $Sr_{0.95}La_{0.05}TiO_3$ ceramic prepared following the same recipe. Reprinted with permission.[12] Please click here to view a larger version of this figure.

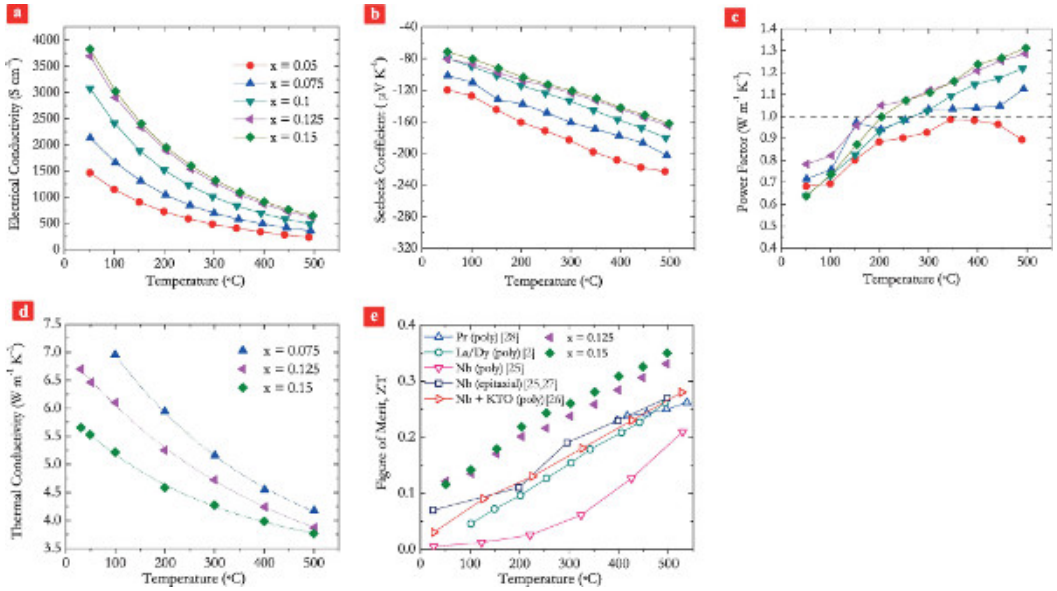

Figure 3. Thermoelectric transport properties. Temperature dependence of (**A**) electrical conductivity (σ), (**B**) Seebeck coefficient (α), (**C**) power factor (defined as PF= α2σT), (**D**) total thermal conductivity and (**E**) figure-of-merit, ZT for $Sr_{1-x}Pr_xTiO_{3-\delta}$ ceramics as a function of Pr content. Temperature dependence of reported maximum ZT values in the literature is shown for comparison.[2,25-28] Reproduced with permission.[12,13] Please click here to view a larger version of this figure.

Discussion

In this protocol, we have presented the steps of the synthesis strategy in order to successfully prepare bulk polycrystalline Pr-doped $SrTiO_3$ ceramics exhibiting improved electronic and thermoelectric properties. The main steps of the protocol include (i) the solid-state synthesis of the doped $SrTiO_3$ powder in air under atmospheric pressure and (ii) taking advantage of the capabilities of spark plasma sintering technique to densify the as-prepared powder into high-density bulk ceramics and at the same time to further dope the grain boundaries of the sample with Pr. It was demonstrated that by applying a high SPS heating rate (300-400 °C min^{-1}) the reflections in the X-ray diffraction patterns corresponding to the secondary phase(s) are fully disappeared (**Figure 1C, D**). The high heating rate is one of the key differences of this synthesis strategy with previous reports in the literature.[17] Complete incorporation of Pr dopants in Sr sites, which lead to measured carrier concentration values corresponding to the nominal doping values[12], is one of the main accomplishments of this synthesis strategy. As a result, higher carrier concentration values were observed for the samples prepared in this work comparing to the values reported in the literature for the samples prepared using other methods with same nominal doping concentrations. Taking advantage of the highly-reducing atmosphere of spark plasma sintering chamber (graphite die under dynamic vacuum and high heating rate) to reduce the oxide powder in order to create oxygen vacancies as another source of electron doping also differentiates this protocol from other samples reported in the literature prepared under Ar[29] or forming gas (5-10% H in Ar)[29] atmospheres.

Furthermore, it was observed that by applying a high SPS heating rate, secondary phases, which are primarily praseodymium oxide, can locally dope the grain boundary regions. This non-uniform doping of the ceramic samples resulted in the observation of an unexpected marked improvement in the carrier mobility, thermoelectric power factor as well as a significant reduction in the total thermal conductivity. The experimental data suggest that the observed enhancement is correlated to the unique microstructure of the ceramics and the presence of Pr-rich boundary regions. Such boundaries were not observed for the $SrTiO_3$ ceramics doped with other dopants such as La (**Figure 2C**, inset) or prepared with other synthesis methods reported in the literature. A recent theoretical study by Dawson and Tanaka attempts to explain this observation (*i.e.,* why Pr-doping induces core−shell formation and La-doping does not) by investigating the local structure and energetics of Pr- and La-doped $SrTiO_3$ grain boundaries.[30] Their calculations show a far stronger energetic benefit for Pr-doping of grain boundaries than La-doping. Since the electronic transport results could not be explained by effective medium theory,[12] it is believed that a charge transfer mechanism is likely to be involved in the carrier mobility improvement.

The results prove that the strategy can be applied as a method to synthesize *in situ* composite structures particularly of the core-shell type structure. However, the efficiency of the non-uniform doping depends on the nature of the constituent phases of the composite. This method is limited by the melting point of the phases present in the material. High heating rates of 300-400 °C min^{-1} can locally melt the material under mechanical pressure and either crack the sample or change the properties. Therefore, this protocol is a good synthesis strategy to be implemented to other oxides due to their high-temperature stability. Caution should be exercised when the method is applied to other thermoelectric materials. The conditions of spark plasma sintering technique need to be optimized before applying the strategy to other materials systems. It should be noted that due to the high heating rates applied, significant grain growth is expected if the densification part of the protocol is employed on nanosctructured powders.

Future work to modify the current protocol in order to further improve the thermoelectric properties will focus on the simultaneous optimization of the effect of the mechanical load (60 MPa in this protocol), the SPS soaking temperature, and soaking time to further reduce the thermal conductivity, improve the power factor, and to improve the success rate of the preparation of crack-free samples.

In conclusion, we have demonstrated the synthesis approach for the preparation of bulk polycrystalline Pr-doped $SrTiO_3$ ceramics with Pr-rich grain boundaries exhibiting significantly improved electronic and thermoelectric properties. The synthesis strategy utilized in this work may open new horizons and opportunities to other properties and applications of this broadly functional perovskite where higher carrier mobility is desired. Moreover, the grain boundary engineering using spark plasma sintering demonstrated in this work can be implemented in other oxide materials to modify the physical properties.

Disclosures

The authors have nothing to disclose.

Acknowledgements

The authors wish to acknowledge the competitive faculty-initiated collaboration (FIC) grant from KAUST.

References

1. Ohta, S., Nomura, T., Ohta, H., Koumoto, K. High-temperature Carrier Transport and Thermoelectric Properties of Heavily La-or Nb-doped SrTiO3 Single Crystals. *J. Appl. Phys.* **97**, (2005).
2. Wang, H. C., *et al.* Enhancement of Thermoelectric Figure of Merit by Doping Dy in La0.1Sr0.9TiO3 Ceramic. *Mater. Res. Bull.* **45**, 809-812 (2010).
3. Bhattacharya, S., Mehdizadeh Dehkordi, A., Alshareef, H. N., Tritt, T. M. Synthesis–Property Relationship in Thermoelectric Sr1−xYbxTiO3−δ Ceramics. *J. Phys. D: Appl. Phys.* **47**, 385302 (2014).
4. Wang, Y., Lee, K. H., Ohta, H., Koumoto, K. Thermoelectric Properties of Electron Doped SrO(SrTiO3)n (n=1,2) Ceramics. *J. Appl. Phys.* **105**, 1037011-1037016 (2009).
5. Wang, N., *et al.* Effects of YSZ Additions on Thermoelectric Properties of Nb-Doped Strontium Titanate. *J. Electron. Mater.* **39**, 1777-1781 (2010).
6. Muta, H., Kurosaki, K., Yamanaka, S. Thermoelectric Properties of Rare Earth Doped SrTiO3. *J. Alloys Compd.* **350**, 292-295 (2003).
7. Shang, P. -P., Zhang, B. -P., Li, J. -F., Ma, N. Effect of Sintering Temperature on Thermoelectric Properties of La-doped SrTiO3 Ceramics Prepared by Sol-gel Process and Spark Plasma Sintering. *Solid State Sciences.* **12**, 1341-1346 (2010).
8. Wang, Y., Fan, H. J. Sr1-xLaxTiO3 Nanoparticles: Synthesis, Characterization and Enhanced Thermoelectric Response. *Scripta Materialia.* **65**, 190-193 (2011).
9. Kikuchi, A., Okinakab, N., Akiyama, T. A Large Thermoelectric Figure of Merit of La-doped SrTiO3 Prepared by Combustion Synthesis with Post-Spark Plasma Sintering. *Scripta Materialia.* **63**, 407-410 (2010).
10. Obara, H., *et al.* Thermoelectric Properties of Y-Doped Polycrystalline SrTiO3.Jpn. *J. Appl. Phys.* **43**, L540-L542 (2004).
11. Koumoto, K., Wang, Y., Zhang, R., Kosuga, A., Funahashi, R. Oxide Thermoelectric Materials: A Nanostructuring Approach. *Annu. Rev. Mater. Res.* **40**, 363-394 (2010).
12. Mehdizadeh Dehkordi, A., *et al.* Large Thermoelectric Power Factor in Pr-Doped SrTiO3−δ Ceramics via Grain-Boundary-Induced Mobility Enhancement. *Chem. Mater.* **26**, 2478-2485 (2014).
13. Mehdizadeh Dehkordi, A., Bhattacharya, S., He, J., Alshareef, H. N., Tritt, T. M. Significant Enhancement in Thermoelectric Properties of Polycrystalline Pr-doped SrTiO3 Ceramics Originating from Nonuniform distribution of Pr dopants. *Appl. Phys. Lett.* **104**, 1939021-1939024 (2014).
14. *Standard Test Methods for Density of Compacted or Sintered Powder Metallurgy (PM) Products Using Archimedes' Principle.* ASTM International West Conshohocken, PA Available from: http://www.astm.org (2015).
15. Parker, W. J., Jenkins, R. J., Butler, C. P., Abbott, G. L. Flash Method of Determining Thermal Diffusivity, Heat Capacity and Thermal Conductivity. *J. Appl. Phys.* **32**, 1679-1684 (1961).
16. Cowan, R. D. Pulse Method of Measuring Thermal Diffusivity at High Temperatures. *J. Appl. Phys.* **34**, 926-927 (1963).
17. Mehdizadeh-Dehkordi, A. An Experimental Investigation Towards Improvement of Thermoelectric Properties of Strontium Titanate Ceramics. *All Dissertations. Paper 1333.* Available from: http://tigerprints.clemson.edu/all_dissertations/1333 (2014).
18. *DSC Pegasus 404C Operating Manual.* Netzsch GmbH Selb, Germany (1999).
19. Daw, J. E. Measurement of Specific Heat Capacity Using Differential Scanning Calorimeter. *Report of US Department of Energy.* Idaho National Laboratory (2008).
20. Tritt, T. M. *Thermal Conductivity: Theory, Properties and Applications.* Kluwer Academic (2004).
21. *SC7610 Sputter Coater Operating Manual.* Quorum Technologies Ltd East Sussex, England Available from: http://www.quorumtech.com/pdf/productOperatingManuals/SC7610_Operating_Manual.pdf (2002).
22. Tritt, T. M. Electrical and Thermal Transport Measurement Techniques for Evaluation of the figure-of-Merit of Bulk Thermoelectric Materials. *Thermoelectrics Handbook: Macro to Nano.* Rowe, D. M. 23(1)-23(17) CRC Press Boca Raton (2006).
23. Burkov, A. T. Measurements of Resistivity and Thermopower: Principles and Practical Realization. *Thermoelectrics Handbook: Macro to Nano.* Rowe, D. M. 22(1) CRC press Boca Raton (2006).
24. *Physical Property Measurement System: AC Transport Option User's Manual.* Quantum Design San Diego, USA Available from: http://www.mrl.ucsb.edu/sites/default/files/mrl_docs/instruments/manPPMS.pdf (2003).
25. Ohta, S., Ohta, H. Grain Size Dependence of Thermoelectric Performance of Nb-doped SrTiO3. *Polycrystals. J. Ceram. Soc. Jpn.* **114**, 102 (2006).
26. Wang, N., He, H., Ba, Y., Wan, C., Koumoto, K. Thermoelectric Properties of Nb-doped SrTiO3 Ceramics Enhanced by Potassium Titanate Nanowires Addition. *J. Ceram. Soc. Jpn.* **118**, 1098 (2010).
27. Ohta, S., *et al.* Large Thermoelectric Performance of Heavily Nb-doped SrTiO3 Epitaxial Film at High Temperature. *Appl. Phys. Lett.* **87**, 092108 (2005).

28. Kovalevsky, A., Yaremchenko, A., Populoh, S., Weidenkaff, A., Frade, J. Enhancement of Thermoelectric Performance in Strontium Titanate by Praseodymium Substitution. *J. Appl. Phys.* **113**, 053704 (2013).
29. Kovalevsky, A. V., *et al.* Towards a High Thermoelectric Performance in Rare-Earth Substituted SrTiO3: Effects Provided by Strongly-Reducing Sintering Conditions. *Phys. Chem.* **16**, 26946 (2014).
30. Dawson, J. A., Tanaka, I. Local Structure and Energetics of Pr- and La-Doped SrTiO3 Grain Boundaries and the Influence on Core–Shell Structure Formation. *J. Phys. Chem. C.* **118**, 25765-25778 (2014).
31. Mehdizadeh Dehkordi, A., *et al.* New Insights on the Synthesis and Electronic Transport in Bulk Polycrystalline Pr-doped SrTiO3−δ. *Appl. Phys. Lett.* **117**, 055102 (2015).

